Development and application of an environmentally friendly ductile alkali-activated composite

Nedeljkovic, M.; Luković, Mladena; van Breugel, Klaas; Hordijk, Dick; Ye, Guang

DOI
10.1016/j.jclepro.2018.01.162

Publication date
2018

Document Version
Accepted author manuscript

Published in
Journal of Cleaner Production

Citation (APA)
Nedeljkovic, M., Luković, M., van Breugel, K., Hordijk, D., & Ye, G. (2018). Development and application of an environmentally friendly ductile alkali-activated composite. *Journal of Cleaner Production*, *180*, 524-538. https://doi.org/10.1016/j.jclepro.2018.01.162

Development and application of an environmentally friendly ductile alkali-activated composite

Marija Nedeljković[a*], Mladena Luković[b], Klaas van Breugel[a], Dick Hordijk[b], Guang Ye[a,c]

[a] Microlab, Faculty of Civil Engineering and Geosciences, Delft University of Technology Stevinweg 1, 2628 CN Delft, the Netherlands
[b] Concrete Structures, Faculty of Civil Engineering and Geosciences, Delft University of Technology, Stevinweg 1, 2628 CN Delft, The Netherlands
[c] Magnel Laboratory for Concrete Research, Department of Structural Engineering, Ghent University Technologiepark-Zwijnaarde 904 B-9052, Ghent (Zwijnaarde), Belgium

e-mail: M.Nedeljkovic@tudelft.nl
M.Lukovic@tudelft.nl
K.vanBreugel@tudelft.nl
D.A.Hordijk@tudelft.nl
G.Ye@tudelft.nl

[*] Corresponding author
Tel: +31(0)15 27 82290

ABSTRACT

This paper presents a development of a ductile alkali-activated fly ash (FA) and ground granulated blast furnace slag (GBFS) based composite as an environmentally friendly material for structural concrete application. For this purpose, polyvinyl alcohol (PVA) fibres and sand aggregate were combined with alkali-activated paste. Workability, setting time, mechanical properties and failure mode of PVA fibres in the mixture were studied by slump test, Vicat needle test, flexural and compression tests, and an Environmental Scanning Electron Microscopy (ESEM) imaging, respectively. Although the mixture sets in a short period of time (less than 30 minutes), the workability was good and the developed fibre reinforced composite was used for a large scale application in a canoe. Casting a large volume

(45 l compared to 3 l, as initially designed) did not affect the workability and the setting time of the mixture. Mechanical properties of specimens coming from “small” (3 l) and “large” (45 l) batches were tested at different ages (up to 120 days) and compared. It was shown that their flexural and compressive strength are similar, i.e. not affected by the upscaling. Furthermore, it was shown that the mixture with PVA fibres exhibits deflection hardening behaviour even with aggregate particles as large as 4 mm, although single crack localization led to failure. The ESEM images of fractured surfaces indicated that combined fibre pull-out and fibre rupture occured, with the latter one causing the final failure. The developed mixture, additionally reinforced with the plastic fiberglass mesh, was used in the 5.8 m long and 16 mm thick canoe for the student competition, which for the very first time, was constructed without the use of Ordinary Portland cement (OPC). The upscaling was successful and the results show the potential of fibre-reinforced alkali-activated FA and GBFS composite to be used as a durable and resistant material suitable for the structural application in thin shell elements, exemplified by the canoe. Such an application and a low risk project was suitable to gain the necessary experience and confidence with this innovative, “concrete like”, material for which no codes or regulations are available. Furthermore, similar applications are the first step for larger scale structural applications, like structural elements in the building industry, bridges and other civil engineering structures.

Keywords: Alkali-activated composite, FA, GBFS, PVA fibres, Ductility, Canoe

1. Introduction

It is well known that concretes using OPC based binders have a negative environmental impact. These materials are unfavourable in terms of CO_2 emission, energy and natural resources consumption (Marinković et al., 2017). The average world carbon intensity of carbon emissions in OPC production is 222 kg of carbon per ton of OPC (Worrell et al., 2001). Considering the molar weight contribution of carbon in CO_2, one ton of OPC results in one ton of CO_2 emission (McLellan et al., 2011). In fact, it is estimated that concrete production is responsible for about 7 % of the global CO_2 output (Kajaste and Hurme, 2016). Large CO_2 emission of concrete industry can be overcome through the replacement of OPC by various industrial by-products, such as fly ash (FA) from coal-fired electricity production and ground granulated blast furnace slag (GBFS) from steel making. These by-products are commonly known as supplementary cementitious materials (SCM) (Lothenbach et al., 2011). When SCM are used with OPC they are activated by $Ca(OH)_2$ that is produced during the hydration of OPC. The amount of $Ca(OH)_2$ for their activation depends on the replacement level of OPC. On the other hand, when used without OPC, no $Ca(OH)_2$ is available for activation and therefore, an appropriate alkali-activator is needed. Composite materials made of alkali-activated FA and GBFS are known as alkali-activated materials (AAM) (Pacheco-Torgal et al., 2014). They are characterized by their low carbon footprint, mechanical properties comparable to OPC concrete, good thermal stability, high chemical and fire resistance (Provis et al., 2015; Provis, 2014). On the other hand, similar to OPC-based binders, AAM are brittle and have relatively poor tensile properties (Sakulich, 2011). These properties can be improved significantly by using fibre reinforcement, whereby the fracture behaviour is changed from brittle to ductile (Naaman, 2007). Furthermore, use of fibres can reduce water demand, shrinkage and microcracking, which is often the problem with GBFS rich alkali-activated binders (Silva and Thaumaturgo, 2003).

The use of fibres in AAM is a new area of research which is gaining increasing attention. Currently, limited literature is available concerning fibre use in AAM or their structural applications. In this work, the effect of different types of fibres and their amount on mechanical properties and the fracture response of AAM is first critically reviewed. Then, a fibre reinforced AAM mixture using PVA fibres is developed. Its efficiency was tested in a (relatively) large but low risk, structural application, namely in making a concrete canoe for a student competition. Finally, recommendations for the future developments of fibre reinforced AAM and their structural applications are given.

2. Literature review

So far in the field of AAM, most researchers focused on using synthetic, e.g. polypropylene (PP), polyvinyl alcohol (PVA) and polyethylene (PE) fibres. For example, Puertas et al. (2000) showed that low fibre content (0.2% in volume) of acrylic and PP fibres did not affect the toughness of different alkaline mortars, while higher content (1%) did result in its improvement.

Zhang et al. (2010, 2012) applied PP fibres and MgO expansive agent in order to mitigate cracking due to drying shrinkage which was observed when more than 10% of GBFS in sodium silicate activated, metakaolin/GBFS based AAM was used. The fibre reinforced AAM coating system showed good anti-corrosion properties and excellent adhesion to OPC-based mortars, which were attributed to the compact microstructure of the material. Namely, the geopolymerization products, unlike the hydration products of OPC, were stable when exposed to cyclic drying/wetting conditions in sea water or exposed in air, giving marine concrete a chemical protection.

Natalie et al. (2011) investigated flexural strength enhancement and increase in toughness of alkali-activated slag (AAS) reinforced by high tenacity (HT)-carbon fibres, commercial E-glass fibres, PVA fibres and polyvinyl chloride (PVC) fibres. They tested

different fibre types while keeping the content (1 wt. % fraction on the total mixture) and the length (7 ± 1 mm length) of fibres constant. Composites reinforced with polymer fibres showed better behaviour compared to those reinforced with glass fibres. PVC and carbon fibres led to the best energy absorption capacity: the post-crack behaviour was significantly improved, resulting in an enhanced ductility of the material after reaching the first cracking strength. Alcaide et al. (2007), however, reported that carbon fibres failed to improve AAS or OPC mortar strength, but did reduce drying shrinkage of AAS by about 50%.

In a more recent study, Choi et al. (2016a, b) compared the mechanical properties of two PE fibre-reinforced, high-strength, ultra-high-ductile composites: AAS-based composite and OPC-based composite. AAS composite showed a higher tensile strain capacity with smaller crack widths and crack spacing compared to the cement-based composite. This can be attributed to the better bond between the matrix and the fibres. However, the AAS composite showed lower compressive and lower tensile strength than the OPC-based composite. Furthermore, the AAS-based composite was found to have a higher (nearly double) ratio of the tensile strength to the compressive strength than the OPC-based composite. They also concluded that a tensile strain capacity and tensile strength of up to 7.50 % and 13.06 MPa, respectively, can be achieved in studied mixtures.

Lee et al. (2012) showed the feasibility of attaining tensile strain up to 4.7% in AAS composite reinforced with PVA fibres. Moreover, Behzad Nematollahi et al. (2015) found low-calcium (Class F) FA-based alkali-activated matrix reinforced with PVA fibres to be highly beneficial in terms of lower cost, higher compressive strength, higher matrix fracture properties, and superior uniaxial tensile behaviour in comparison to engineered cementitious composite. The FA-based alkali-activated composite exhibited compressive strength, tensile strength and maximum tensile strain of 60 MPa, 4.7 MPa, and 4.3% on average, respectively.

Silva et al. (2003) studied fracture response of alkali-activated and OPC mortars, reinforced with different volumes (V_f=0 to V_f=5%) of natural wollastonite microfibres. First, they found that the toughness difference between alkali-activated and OPC mortars without fibres is about 80%. The maximum toughness in both composite systems with fibres was achieved with 2% of fibres by volume. The relative toughness of alkali-activated and OPC mortars reinforced with 2% of fibres by volume, increased by 60% and 40%, respectively, compared to their corresponding mixtures without fibres. Higher volumes of fibres lead to decrease in toughness due to an increase in porosity.

Basalt fibres in alkali-activated concretes showed to be beneficial, which is not always the case with the tested OPC-based mixtures. Namely, Dias and Thaumaturgo (2005) compared performances between alkali-activated and OPC concretes reinforced by these fibres. While in OPC concrete this had an adverse effect, addition of basalt fibres in alkali-activated concretes led to increased tensile strength compared to reference mixtures without fibres (34% for Vf=0.5% and 25% for Vf=1.0%). Beneficial effects of basalt fibre addition on energy absorption, were reported by Li and Xu (2009a, b), who studied the impact properties of sodium silicate activated slag/fly ash blends.

The use of steel fibres was also attempted in AAM. Bernal et al. (2010) investigated AAS-based concrete reinforced with 40 kg/m^3 and 120 kg/m^3 of steel fibres. They found that the water absorption coefficient and permeability were markedly reduced with the addition of the fibres, compared to the reference AAS-based concrete. Both splitting tensile and flexural strengths were largely improved with increasing fibre volume. However, the compressive strength was reduced.

In Table 1, the main benefits and drawbacks of fibre reinforced AAM are summarized. Researchers used diverse ways to develop fibre reinforced AAM and fibres were mainly applied to control cracking, increase strength and durability. In practical engineering

applications, it is of paramount significance that fibre reinforced AAM can be successfully applied in structures considering their rapid hardening and loss of workability. In addition, there is a lack of information and no available codes related to upscaling of fibre reinforced AAM from laboratory to larger scale structural applications, something that has already showed to be a challenge in applications of the fibre reinforced OPC concrete. The final limitation to wide structural application of AAM is that, so far, no international codes or regulations are available nor there are experience and confidence in their long-term behaviour.

Apart from developing an environmentally friendly ductile alkali-activated FA and GBFS composite, another important aim of this study was to upscale it for practical, structural application. In order to improve the ductility and fracture behaviour of AAM, and to mitigate the risk of shrinkage cracking, PVA fibres are used. The mechanical properties of alkali-activated FA and GBFS composite cast in two batch sizes (3 litres and 45 litres) at different curing ages are compared. In addition, the rheological and microstructural properties of samples from different batches are analysed. Finally, in a field test, a canoe made from the developed mixture is successfully tested, proving its structural capacity and water tightness.

Table 1 Summary of the main benefits and drawbacks of fibre reinforced AAM.

Ref	Fibre type	Benefits	Drawbacks
(Aydın and Baradan, 2013)	steel	-improved compressive and, flexural strengths -improved toughness -reduced drying shrinkage	-decreased workability
(Bernal et al., 2010)	steel	-improved absorption and permeability -improved splitting and flexural strengths	-decreased compressive strength
(Zhang et al., 2010; 2012)	polypropylene	-suitable setting time, high bond strength and excellent anti-corrosion properties, -large shrinkage during setting and hardening	-decrease resistance to marine environment

		reduced by adding MgO-based expansion agent and PP fibres	
(Puertas et al., 2003)	polypropylene	-improved impact resistance after wet/dry cycles -reduced drying shrinkage of the specimens cured at 21 ºC and 50 % RH	-decrease modulus of elasticity -increase drying shrinkage of the specimens cured at 95 % RH
(Choi et al., 2016a)	polypropylene	-alkali-activated GBFS-based composite showed a higher tensile strain capacity than the cement-based composite	-lower compressive strength
(Choi et al., 2016b)	polypropylene	-average tensile strength to compressive strength ratio was double that of normal concrete	
(Lee et al., 2012; Nematollahi et al., 2015)	polyvinyl alcohol (PVA)	-improved ultimate tensile strain - improved compressive strength	
(Natali et al., 2011)	High tenacity-carbon polyvinyl chloride (PVC)	-improved adhesion properties of coating -improved post-cracking behaviour and enhanced the ductility -the maximum flexural strength was achieved for high tenacity-carbon -improved energy absorption capacity	
(Natali et al., 2011)	E-Glass polyvinyl alcohol (PVA)	- improved adhesion properties of coating	
(Li et al., 2009a, b)	basalt	-improved energy absorption capacity	-no effect on the dynamic compressive strength
(Dias and Thaumaturgo, 2005)	basalt	-superior load capacity and fracture toughness of alkali-activated concretes	
(Alcaide et al., 2007)	carbon	-reduced drying shrinkage	-no effect on the compressive strength
(Puertas et al., 2006)	glass	-reduced shrinkage	-no effect on the mechanical properties

(Silva and Thaumaturgo, 2003)	wollastonite microfibres	-improved fracture toughness

3. Materials and methods

3.1. Materials

3.1.1. Ground granulated blast furnace slag and fly ash

The GBFS and FA were used as a raw material in the mixtures. GBFS was supplied from ORCEM, and FA by VLIEGASUNIE BV, both from the Netherlands. X-ray fluorescence (XRF) measurements were done using a PANalytical's Epsilon 3^{XLE} spectrometer equipped with a Rhodium X-ray source, the silicon-drift detector with 135 eV resolution at 5.9 keV/1000 cps. The chemical compositions of GBFS and FA, measured by XRF are shown in Table 2.

Table 2 Chemical composition of GBFS and FA measured by XRF [%].

	SiO_2	Al_2O_3	CaO	MgO	Fe_2O_3	S	Na_2O	K_2O	TiO_2	P_2O_5	L.O.I.
GBFS	35.5	13.5	39.8	8.0	0.64	1.04	0.4	0.53	1.0	0.009	-1.3
FA	56.8	23.8	4.8	1.5	7.2	0.3	0.8	1.6	1.2	0.51	1.2

Fig. 1 shows the particle shape of GBFS and FA, studied by scanning electron microscope (ESEM-BSE), Philips-XL30-ESEM. The GBFS particles have clear edges and angles. On the other hand, FA particles consist of individual and agglomerated glassy spheres. The mean particle size of GBFS, d_{50}, was 19 μm, while for FA, d_{50} was 54 μm, as determined by EyeTech Laser diffraction analyser, Ankersmid.

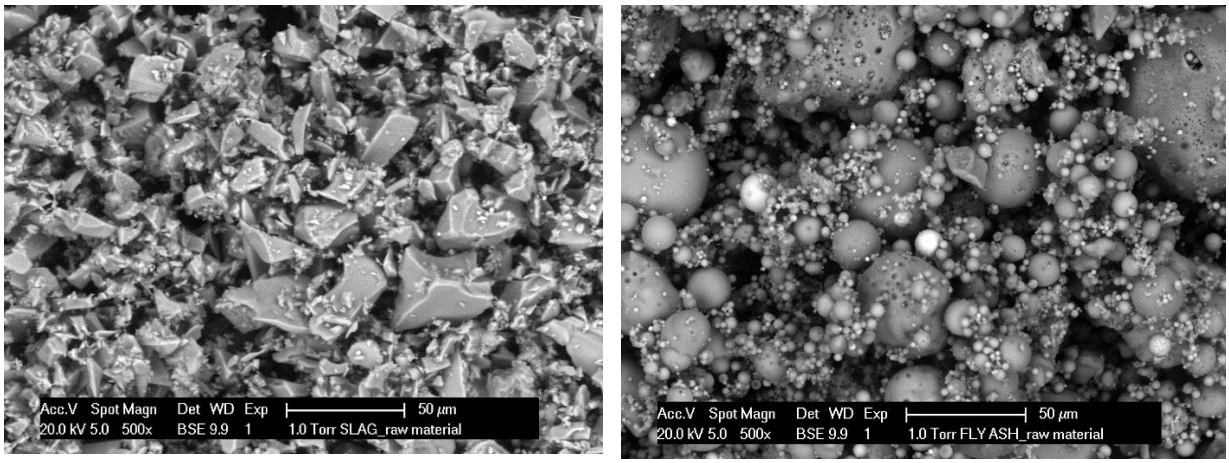

Fig. 1. ESEM-BSE images of GBFS (left) and FA (right) particles.

3.1.2. Aggregate

In order to enhance fibre bridging capacity, fibre reinforced composites are usually designed with smaller size aggregate fraction (Paul et al., 2013). This is also desirable for the aforementioned application of the developed AAM in thin shell elements, considering that the designed thickness of the canoe was 16 mm. Therefore, in the developed mixture, sand distribution is conforming the grading limits in range 0-4 mm. The used sand aggregate has specific gravity of 2640 kg/m^3 and water absorption of 3.75 %.

3.1.3. Alkaline activator and superplasticizer

The alkaline activator was prepared by mixing sodium hydroxide (analytical grade, >98 % purity) with distilled water and sodium silicate solution (SiO_2: 27.5 wt. %, Na_2O: 8.25 wt. %). The activator was left for 24 h after mixing at room temperature prior to preparation of the samples. The activator to binder ratio in the fibre reinforced mortar was 0.45. A sodium naphthalene formaldehyde sulphonate-based superplasticizer of 0.14 wt. % by binder (FA and GBFS together) was used to improve the workability. The naphthalene-based superplasticizer was chosen because of its inherent stability in alkaline media (Palacios et al., 2008).

3.1.4. Fibres

In line with the literature study on fibre reinforced AAS, in this study PVA fibres with a length of 8 mm and a diameter of 40 μm were used. The tensile strength of the PVA fibre is 1600 MPa and the density is 1300 kg/m^3. The amount of fibres added to the mix is 2 % by the total volume of the composite. This is in accordance with percentages commonly used in strain hardening cementitious composites (SHCC) (Li, 2003; Zhou et al., 2010).

3.1.5. Mix proportioning

Previous results (Nedeljković et al., 2016) indicated that increase of GBFS in FA/GBFS based binder decreases the final setting time and increases the compressive strength of alkali-activated pastes. In this respect, FA to GBFS ratio of 1:1 led to the optimal performance and volume stability of alkali-activated pastes: on one hand, this mixture has longer initial setting time and it was less brittle compared to the one with higher GBFS content; on the other hand, it showed higher strength compared to the mixtures with lower GBFS content. Therefore, the ratio of FA to GBFS of 1:1 was used in the mixtures. As a reference to fibre reinforced alkali-activated mortar, alkali-activated paste and non-fibre reinforced mortar were also made (Table 3). Based on the previously developed SHCC mixtures (Zhou et al., 2010; Lukovic, 2016), the sand content of 30 % by volume was used in this research. The amount of superplasticizer was 0.14 wt. % of binder. First, a control mix of 3 litres was tested. For large-scale applications, the same mix was cast in a 45 litres batch to ensure that the properties of the material can be retained in "real" application, which is always a concern when fibres are added and large batches of AAM are cast. Material properties for the two batches are further compared.

Table 3 Mixture design for paste, mortar and fibre reinforced mortar [m^3].

	Paste	**Mortar**	**Fibre**

		[m^3]	[m^3]	**reinforced mortar** [m^3]
Components:	Density [kg/m^3]	Mass [kg]	Mass [kg]	Mass [kg]
Fly ash	2440	645	373	437
Blast furnace slag	2890	645	373	437
Aggregate [0-2 mm]	2650	-	1119	-
Aggregate [0-4 mm]	2650	-	-	775
Alkaline activator	1125	645	373	393
Superplasticizer	1070	-	-	1.4
PVA fibres	1300	-	-	26

3.1.6. Mixing and curing

A HOBART mixer was used for mixing 3 litres batch. Aggregate, FA, GBFS and fibres were premixed in this mixer for 3 min at low speed. For mixing the 45 litres batch, forced pan type mixer (Zyklos) with the maximum capacity of 120 litres was used. Irrespectively of used mixer, after premixing raw material and fibres, alkaline activator and superplasticizer were added at low speed mixing. Mixing continued at low speed for 1 min and then at high speed for 2 min. The mix was cast in plastic cubes (40x40x40 mm^3), coupon specimens (240x60x10 mm^3), and prisms (400x100x100 mm^3). Samples were demoulded 24 h after casting and further cured in a fog room at 22°C and RH ~ 99 %.

3.2. Experimental methods

3.2.1. Testing of fresh properties

Properties of fresh mixtures were determined by testing workability, setting time and density in the fresh state. The workability was measured by a mini-slump spread test (Li and Ding, 2003). In this test, the fresh mixture was poured into a slump cone with a top diameter of 36 mm, a bottom diameter of 60 mm and a height of 60 mm. The cone was placed in the centre of a square glass plate. After filling it with the material, the cone is lifted and the mixture

subsides. After one minute, the average spread of the mixture, as measured along the two diagonals and two median directions, was recorded. The setting time of mixtures was determined by the Vicat needle method according to NEN-EN 196-3 (2005). The density was measured in accordance with NEN-EN 12350-6 (2009).

3.2.2. Testing of hardened properties

Four sets of tests were done for investigating and comparing the hardened properties of mixtures cast in two batch sizes (small 3 litres and large 45 litres): the compression test on 40x40x40 mm^3 cube samples, three-point bending test on 40x40x160 mm^3 specimens, the four-point bending test on 30x10x120 mm^3 specimens (Fig. 2a) and three-point bending test on 100x100x400 mm^3 specimens (Fig. 2b). Flexural strength and deflection capacity were determined from the four-point bending test. The hardened properties were tested at the age of 1, 3, 7, 28 and 120 days.

Beside the four-point bending test, the mixture cast for the large batch was also tested in three-point bending tests in accordance with NEN-EN 14651+A1 (2005) (Fig. 2), with the exception that the specimen size was modified and tests are done on 100x100x400 mm^3 prisms (instead of standard cross section of 150x150 mm^2 with a length between 550 to 700 mm). The reason for modification of the sample size was the size of the available moulds. The main goal of this experiment was to see if in the thicker samples, different fibre orientation would have the effect on the measured flexural strength compared to the thinner samples. Therefore, this modification of the specimen size was considered acceptable. First, a notch of 25 mm was made in the middle of all the samples. Then, the samples were left to dry for 2 hours before the three-point bending test was performed. The test was done using horizontal displacement over the length of 50 mm at the tip of the notch as a control, which enabled the analysis of the post-peak behaviour. Samples were tested at the age of 7 and 120 days.

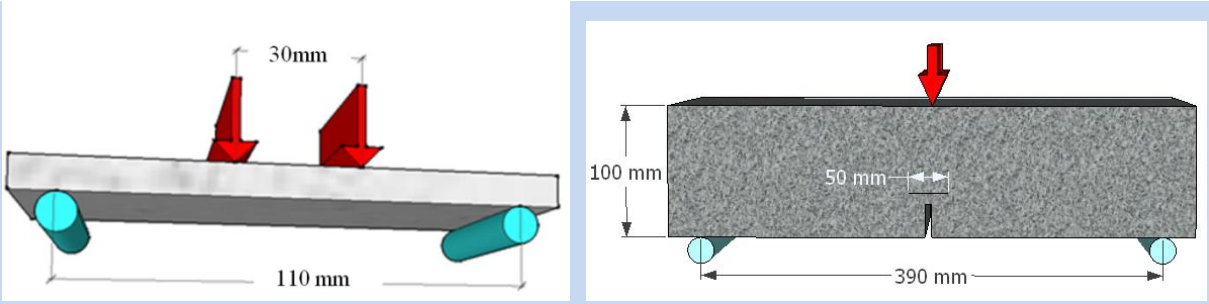

Fig. 2. Flexural tests: a) four-point bending test, b) three-point bending test on notched sample.

3.2.3. Microscopy

To examine the effects of adding PVA fibres on fracture behaviour of fibre reinforced AAM, the microstructural observations and imaging of fracture surfaces of fibre reinforced alkali-activated composites after four-point bending test were performed using Leica MZ6 modular stereomicroscope and Philips-XL30-ESEM under a high-vacuum chamber condition. The ESEM imaging was done in SE (secondary electrons), BSE (back-scattered electrons) and combined SE and BSE conventional modes. Prior to electron microscopy tests, samples were carbon coated.

4. Results and discussion

4.1. Fresh properties

4.1.1. Workability

During testing of the fresh behaviour of mixtures, no bleeding was observed for any of the batch sizes. Slump spread diameter was 105 mm and 130 mm, for 3 litres and 45 litres batch, respectively. The 45 litres batch was more flowable compared to 3 litres batch, and therefore the spread diameter has increased. This provided additional time prior to the initial setting during making of the canoe. Furthermore, the mixture had good filling ability due to the increased volume and spherical shape and smooth glassy surface of FA particles (Fig.1.)

resulting in high fluidity of the alkali-activated FA and GBFS mortar, which was suitable for casting in the thin concrete shell structure such as a canoe (Fig. 3). The final application of the mixture in a canoe will be discussed more in Section 5.

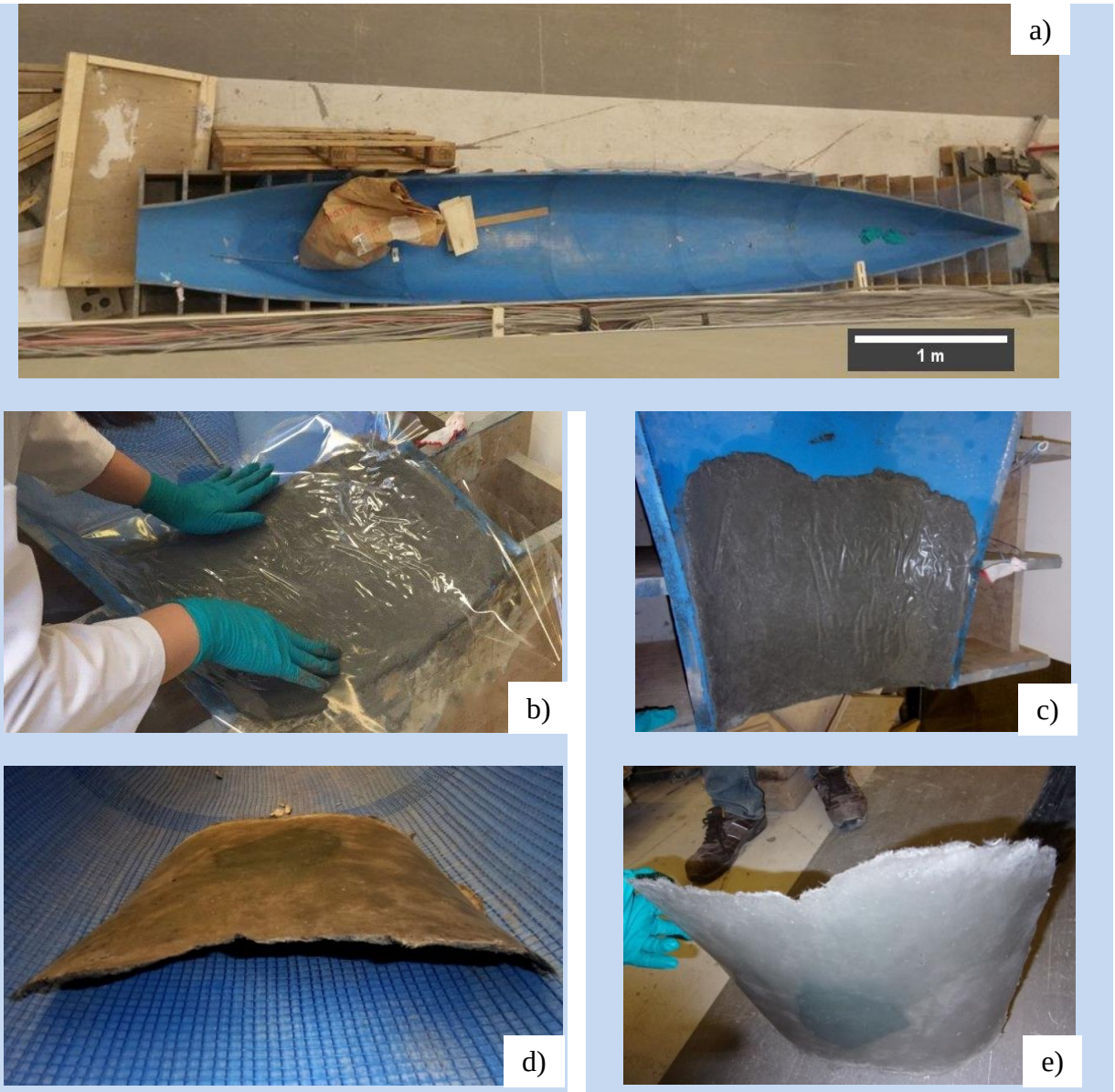

Fig. 3. a) Photograph of the canoe mould (length of 5.8 m, width of 0.73 m), b) casting the trial layer in the canoe mould, the layer was covered with plastic sheet, c) after the initial setting, d) top view of the layer (after 1 hour of curing), e) side view of the layer.

4.1.2. Density and setting time

The theoretical density calculated from mix design was 2.1 g/cm^3, whereas the measured density was 2.02 g/cm^3. Regarding the small difference between measured and calculated values, these results show that the fibre reinforced alkali-activated composite was satisfactorily handled during the mixing procedure described in Section 3.1.6. Setting times for mixtures are reported in Table 4. In general, the setting time depends on precursors and composition of alkaline activators. In alkali-activation process, the high alkalinity of the activator first leads to the release of silicon, aluminium, calcium from the FA and GBFS. The species that are released from the glassy particles then diffuse through the exterior layer of reaction products which rapidly forms around the unreacted FA and GBFS particles. The alkaline conditions accelerate the process of activation, as the presence of hydroxide enhances GBFS dissolution, and also increases the solubility of silica and alumina. In the alkali-activated paste, GBFS particles are dissolved in a short period of time and subsequently start to harden resulting in a short initial setting time (Table 4). However, initial setting time of the composite with PVA fibres, aggregate and superplasticizer is delayed. Paste is the component that sets and using any other inert component in the mix can retard the reaction. This can be considered beneficial for structural applications of the material, because it enables more time for handling and placing of the fresh material.

Table 4 Setting time of alkali-activated: paste and fibre reinforced mortar.

	Alkali-activated paste without fibres w/b=0.5	Fibre reinforced alkali-activated mortar w/b=0.45
Initial setting time	15 min	24 min
Final setting time	28 min	40 min

4.2. Hardened properties

4.2.1. Compressive and flexural strength

The purpose of the compression tests was first to evaluate the effect of addition of aggregates, and then to evaluate the effect of addition of both aggregates and fibres to the alkali-activated FA and GBFS paste. Therefore, compressive strength of the paste, standard mortar and fibre reinforced mortar, based on the same alkali-activated binder is compared. The activator to binder ratio for paste and standard mortar was 0.5. However, experiments carried out with ratio of 0.5 in the fibre reinforced mortar have shown that the mix was too fluid and difficult to stick to the wall of the canoe mould. To avoid bleeding the activator to binder ratio in fibre reinforced mortar was reduced (from 0.5 to 0.45). Furthermore, to enhance its workability, superplasticizer was added to the binder. The results are shown in the Fig. 4.

Compressive strength of the standard mortar is slightly lower compared to the paste for all testing ages (Fig. 4). This is most likely due to the presence of Interfacial Transition Zone (ITZ) around aggregate particles in mortar. The phenomenon of relatively weaker ITZ zone in OPC-based materials arises, at least in part, due to the spatial distribution of cement grains against the larger aggregate particles (the so-called wall effect) (Scrivener et al., 2004). Such packing leads to a more porous area around the aggregates, leading to reduction of the overall mortar strength compared to the strength of the corresponding pastes. A similar phenomenon is observed in this study regarding the difference in strength between alkali-activated paste and mortar samples.

Although the applied activator to binder ratio was lower compared to the paste, the fibre reinforced composite results in an even lower compressive strength compared to that of the standard mortar at the same age. It is assumed that lower compressive strength of fibre reinforced alkali-activated composite is due to its higher porosity compared to denser paste or

nonreinforced mortar, such as reported for OPC composites (Jiang et al., 2014), where the addition of fibres is known to lead to an increased porosity.

The compressive strength development for the same fibre reinforced mixture cast in two batches of 3 litres and 45 litres is shown in Fig. 5. A general trend that compressive strength for 45 litres batch is lower than that of 3 litres batch is observed, with the exception for the first day compressive strengths, for which the difference is within the standard deviation and is attributed to data scatter. Lower compressive strength of the "large" mixture compared to the "small" one can be attributed to the upscaling process, i.e. to the effect of the packing density of the fine aggregate, and their water absorption capacity to take up more water during the initial mixing stage of large batch compared to mixing of batch of 3 litres. The higher porosity, in the hardened composite of larger mixture can be expected. Another possibility is the clustering of fibres in "large" mixture, which are more difficult to be uniformly distributed compared to the "small" mixture. However, the strength development of the studied mix volumes follows the same trend.

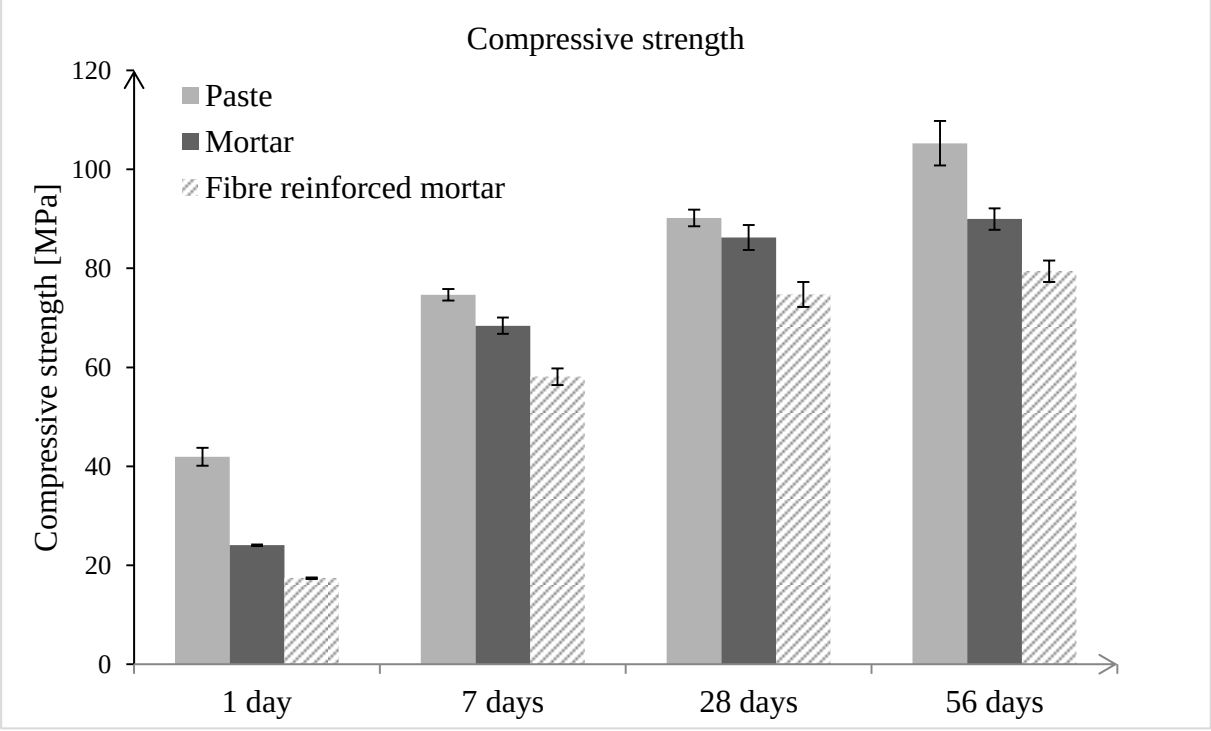

Fig. 4. Compressive strength of the pastes, mortar and fibre reinforced mortar based on alkali-activated FA and GBFS.

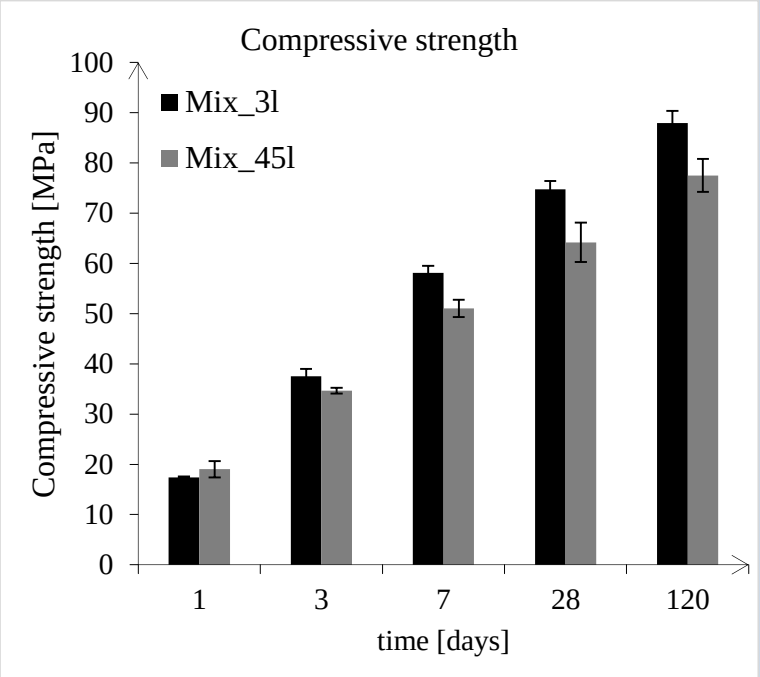

Fig. 5. Effect of the mixture content on the compressive strength of the fibre reinforced alkali-activated composites, 3 litres and 45 litres.

Contrary to the tendencies in compressive, flexural strength of the paste is lower than that of the mortar (Fig. 6). One of the reasons might be that the paste, due to the shrinkage and higher brittleness, probably has more interconnected microcracks, which eventually reduces tensile (and flexural) strength but does not have a significant effect on compressive strength. In the case of mortar, these microcracks are easier interlocked and stopped by stiff sand inclusions (Luković et al., 2016), resulting in more tortuous and discontinuous cracks, which have less effect on the tensile (and flexural) strength of the mortar. Similarly, due to the fibre bridging properties, shrinkage induced microcracking has even less effect on the tensile strength of the fibre reinforced mortar.

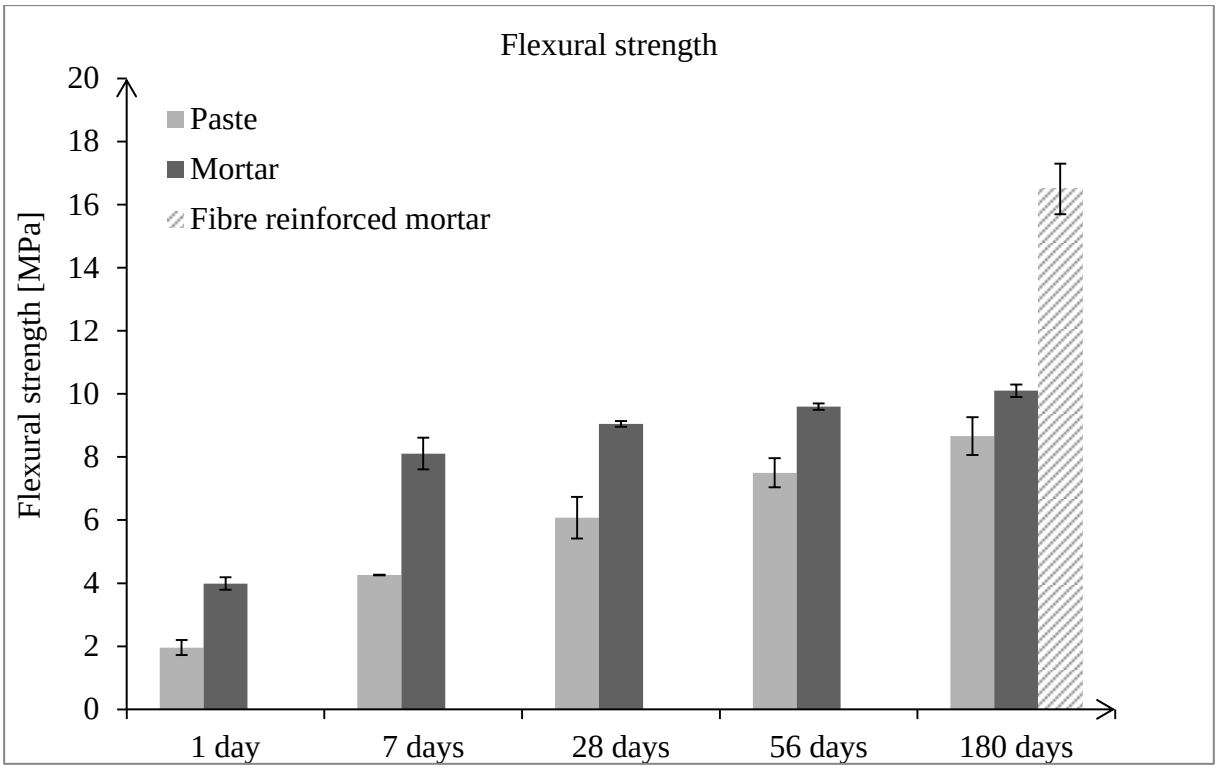

Fig. 6. Flexural strength of the pastes, mortar and fibre reinforced mortar based on alkali-activated FA and GBFS, measured by three-point bending test on samples 40x40x160 mm^3.

4.2.2. Flexural strength by four-point bending tests (batches of 3 litres and 45 litres)

The flexural stress–displacement curves for the two batches based on the PVA fibre-reinforced alkali-activated FA and GBFS at 1, 3, 7, 28 and 120 days are presented in Fig. 7. As commonly observed in fibre reinforced OPC-based composites, in fibre reinforced AAM as well, the strength generally increases but the ductility decreases over time.

Unlike plain concrete, a fibre-reinforced concrete specimen might not fail after localization of a single crack. Instead, once a crack opens, fibres take over the entire tensile force at the location of the crack (Fig. 8). If the force that can be withstood increases, with the condition that the fibres at the location of the crack do not rupture nor are pulled-out, a new crack at another location in the specimen might open. Consequently, the fibres at that location will be activated and will transfer the force (Mehta and Monteiro, 2006; Shah, 1991). This process

creates conditions for multiple cracking which will continue until either the fibres at the location of cracking fail or they are pulled out from the matrix. In the load-deflection curve this behaviour is commonly recognized by the strength increase over deflection (or strain), when the first cracking strength is higher than the peak strength. This is commonly referred as deflection (or strain) hardening behaviour.

Still, although curves in Fig. 7 clearly indicate deflection hardening, from the crack pattern, only one (visible) crack can be observed (Fig. 8). Achieved ductility and hardening behaviour in this case is therefore probably due to a small sliding of the fibres over the total volume. In addition, the main crack is not straight, so the tortuosity of this crack in combination with the high fibre pullout strength can also contribute to the observed deflection hardening behaviour even though a single crack is present.

Generally, fibre pullout, rather than fibre rupture, is more beneficial in order to increase the ductility of fibre reinforced composites (Li and Stang, 1997). Considering high bond strength between fibres and AAM, in order to prevent fibre rupture and therefore enhance the microcracking behaviour and the ductility, high strength fibres, such as polyethylene or aramid fibres, used for designing high strength strain hardening cementitious composite (HS-SHCC) (Curosu et al., 2016; Curosu et al., 2017), might be more promising compared to PVA fibres. Results of flexural strength for both 3 l and 45 l samples presented in the Fig. 7 are similar at the different tested ages. However, it was observed that at the age of 7 days, the flexural strengths of 3 l samples were significantly higher than that of 45 l samples (Fig. 7 and Fig. 9). The reason is unclear, although it may be a result of sample preparation or testing conditions. At other curing ages (1, 3, 28, 120 days), the results are similar for both 3 l and 45 l samples. This will be further investigated in the future. Similarly, the flexural deflection capacity, presented in Fig. 10, confirms the general trend of reduced ductility over time, but

the change in trend after 7 days for 3 litres and 45 litres mixes is not clear, and should be further investigated.

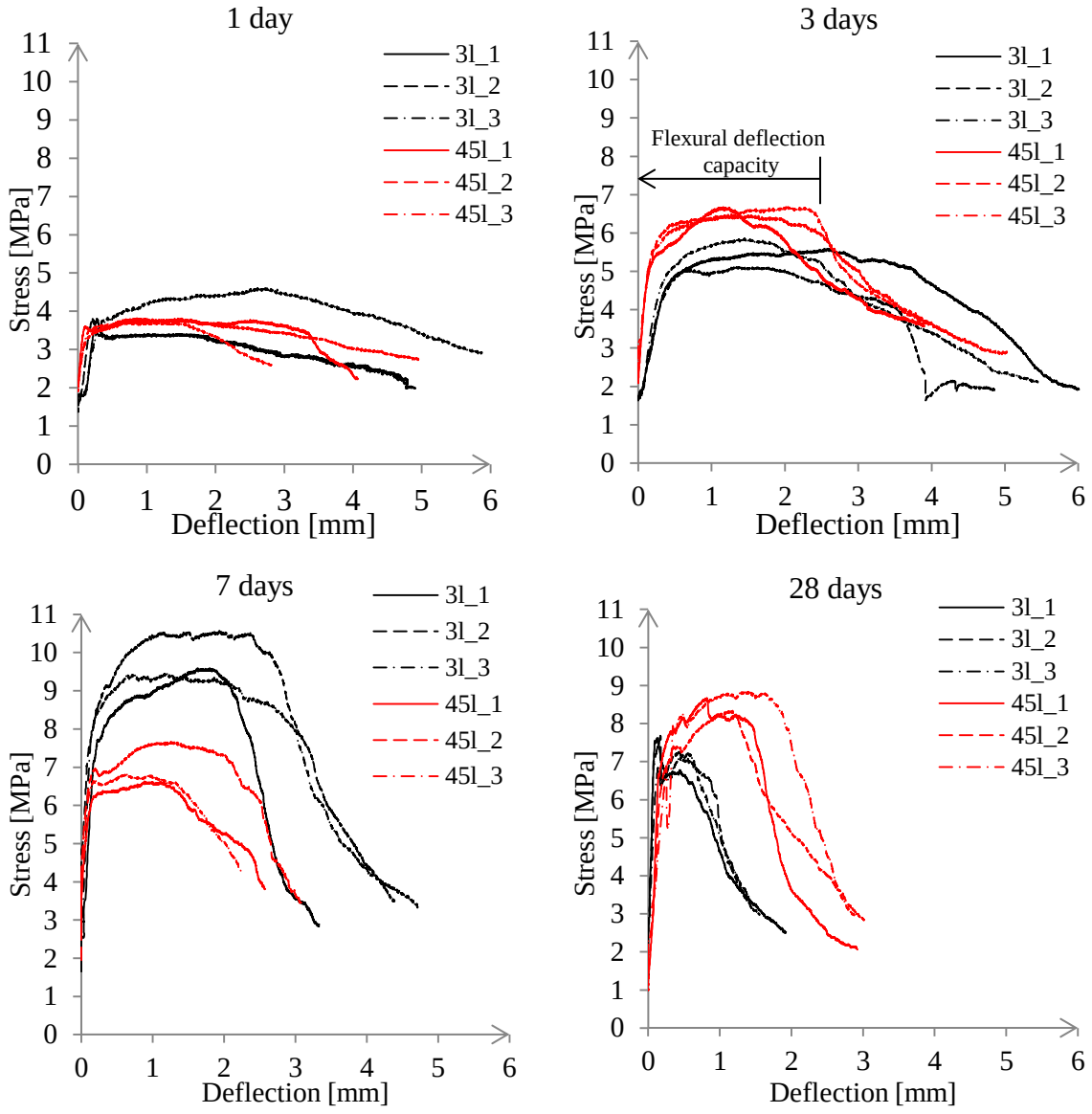

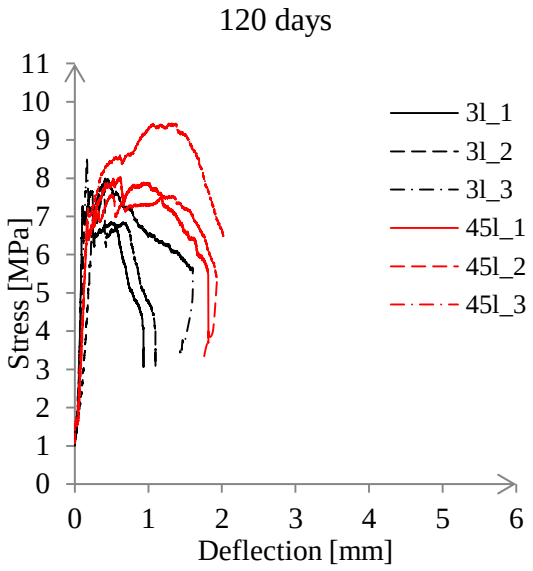

Fig. 7. Flexural load-displacement curves for 3 litres (black) and 45 litres (red) after different ages (1, 3, 7, 28 and 120 days).

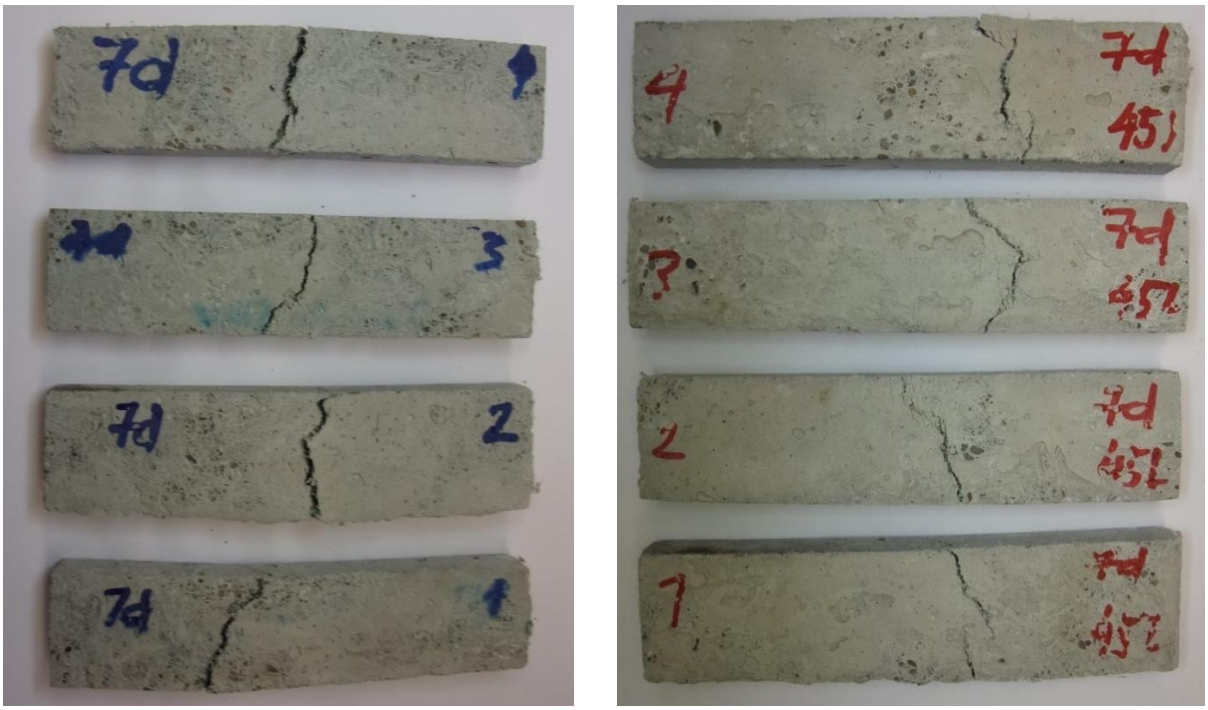

Fig. 8. Crack patterns for mix 3 litres (left) and mix 45 litres (right) after 7 days of curing on samples tested in four-bending test.

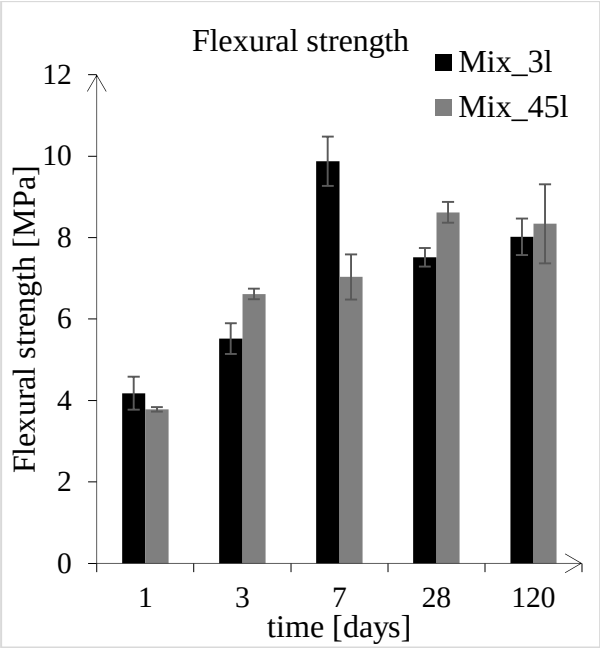

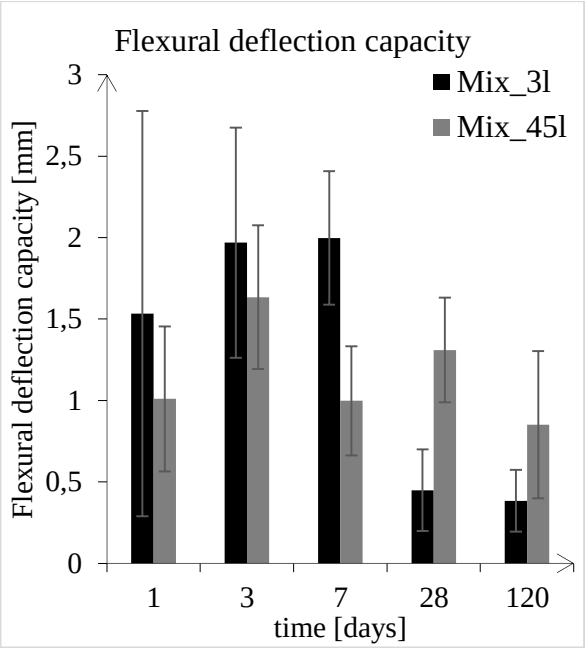

Fig. 9. Flexural strength of the 3 litres and 45 litres samples (10x30x120 mm^3), measured by four-point bending tests.

Fig. 10. Flexural deflection capacity of the 3 litres and 45 litres samples at the maximum load (defined according to Fig. 7).

4.2.3. Flexural strength by three-point bending tests on the notched samples

Fibre reinforced material cast in small thickness samples shows superior behaviour over thicker samples due to the preferential fibre alignment. Namely, in thinner samples, fibres are preferentially oriented in the horizontal direction and have an almost 2D orientation, which is beneficial for strain/deflection hardening behaviour and high ductility. In the French regulations for Ultra High Performance Fibre Reinforced Concrete (UHPFRC) (AFGC, 2013) this effect is also recognized and the problem is addressed by defining two different types of tests: using both thin and thick elements. Furthermore, in the Model Code 2010 (2013) size dependent fibre orientation and applied casting procedure in actual structures are addressed by introducing a fibre orientation factor (so-called K factor). In order to determine this factor, the French Association for Civil Engineering Group (AFGC, 2013) prescribes the use of suitability (control) test in conditions representative of the real structure (the same element thickness, casting procedure, etc.). K factor is then defined as the ratio of the peak load

obtained with the cast prism (used to determine the intrinsic post-cracking law) to the peak load obtained on sawn specimens (taken from the actual structure). This factor is then further used to adjust the constitutive laws and optimise the structural design. The tested thickness of the sample in this study was 10 mm while the thickness of one canoe layer was 8 mm (the canoe was cast out of the two layers as explained later). Therefore, the thickness of the tested (i.e. "thin") sample and the actual structural member were close. Even more, due to the reduced size of the actual member and consequently more preferential fibre orientation, if values presented in Fig. 9 and 10 are used, calculations are on the safe side. In order to check the scale effect of fibre orientation for future applications of the developed mixture, three-point bending tests were done also on big notched specimens (100x100x400 mm^3, with the thickness of 75 mm at the location of the notch). Stress displacement curves are given in Fig. 11a and confirm that deflection hardening is achieved even in the bigger specimens. In addition, compared to flexural strengths of thin samples (Fig. 11b) there is no significant scale effect (Fig. 11a). The crack patterns at the notch after three-point bending test for mixture 45 litres at 7d and 120d are shown in Fig. 12. The crack directions were observed to be different at the tested curing ages. At 7 days crack developed under an angle, while at 120 days it was parallel with the direction of the applied load. Note that at 120 days, only one specimen has been tested, so this result can be considered merely as the indication.

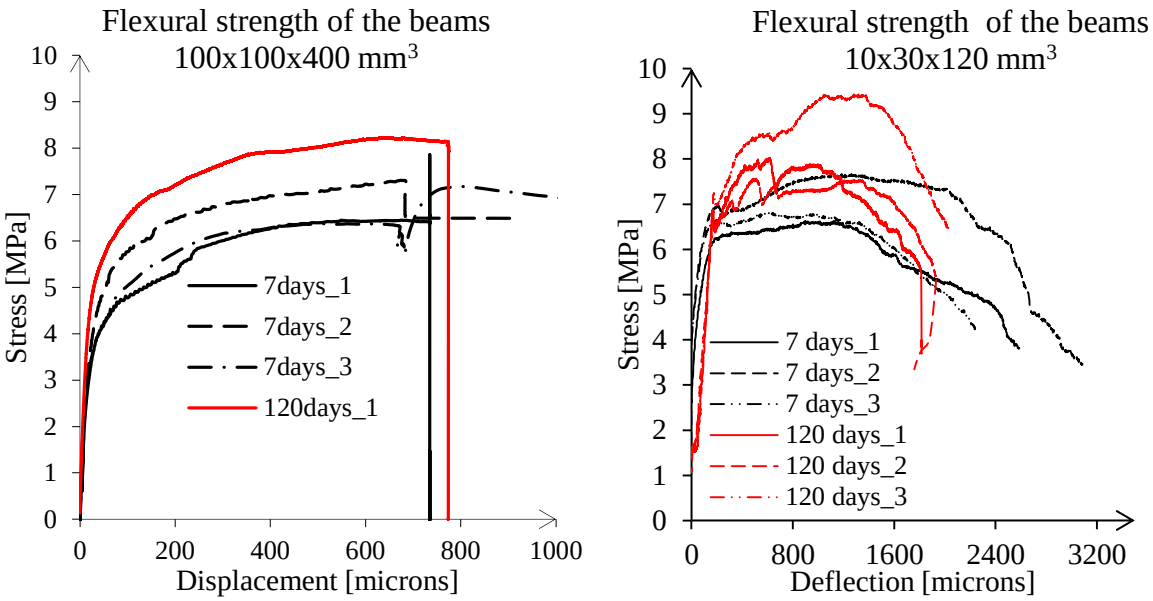

Fig. 11. Flexural tests on (a) 100x100x400 mm^3 notched samples (left) and (b)10x30x120 mm^3 notched samples (right) made from 45 litres batches at 7d and 120d.

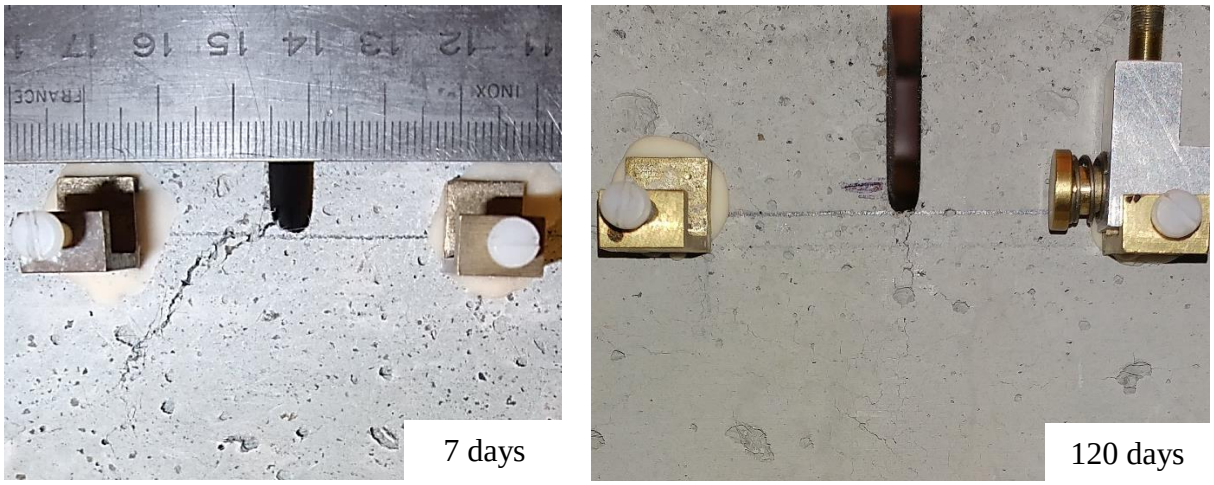

Fig. 12. Crack patterns at the notch after three-point bending test for mixture 45 litres at 7d and 120d.

4.3. Microscopy

The combined light and electron microscopy (ESEM) imaging was performed to study the distribution of PVA fibres in the alkali-activated composite and ultimate fracture in a specimen in the bending tests. To examine fractured surfaces, the bond between matrix and fibres which is influenced by the microstructure of the material, needs to be understood. As

soon as a crack arises, the fibres at that location are pulled, resulting either in the debonding or rupturing. This effect was intended to be seen under the light microscope as shown in Fig. 13. It can be observed that the most of the fibres are partially pulled out, but that the specimen finally failed due to fibre rupture.

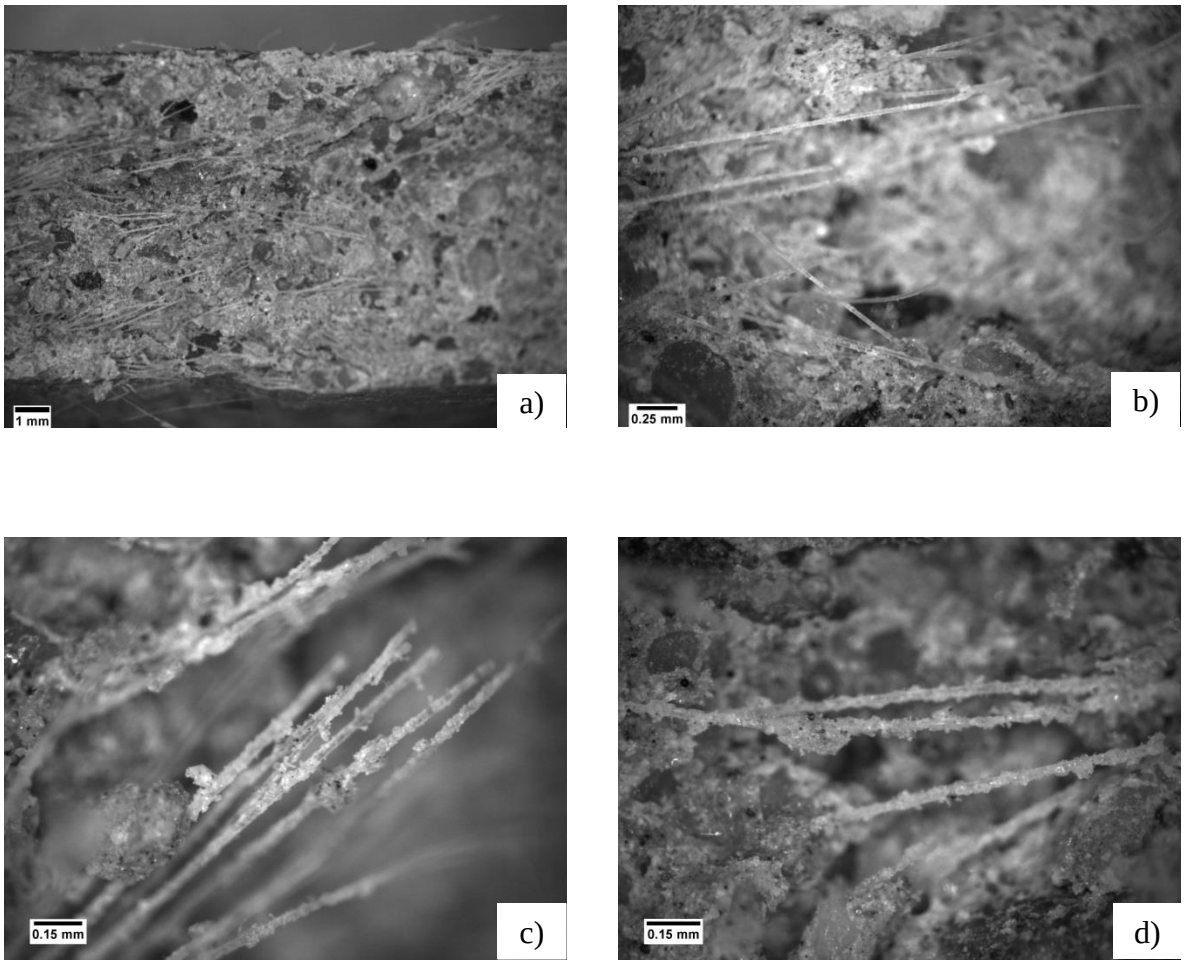

Fig. 13. Optical micrographs of the fractured samples at 120 days a) Top surface of the fractured sample (0.63x magnification), b) Fiber pullout and fiber-matrix debonding (2x magnification, c) Fiber pullout magnified (4x magnification), d) Fiber bridging and fiber-matrix debonding (4x magnification).

Fig. 14 shows the representative ESEM images for PVA fibre-reinforced alkali-activated specimens tested at the age of 120 days. The bond between PVA fibres and the alkali-activated FA and GBFS matrix is observed in different modes. It is clear that fibre pullout and fracture (refer to light microscopy photos of Fig. 13) are the main mechanisms that lead to the enhanced tensile (and flexural strength) and ductility, which is in accordance with the

description by Savastano et al. (2005) for OPC fibre composites. Closer scanning shows that PVA fibres have good bonding with the matrix as many of them are finally ruptured.

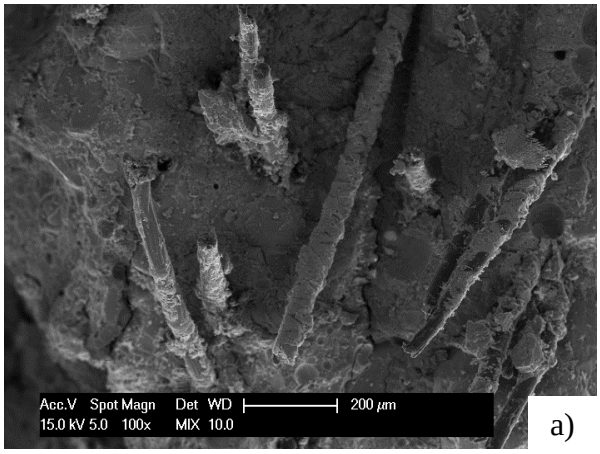

a)

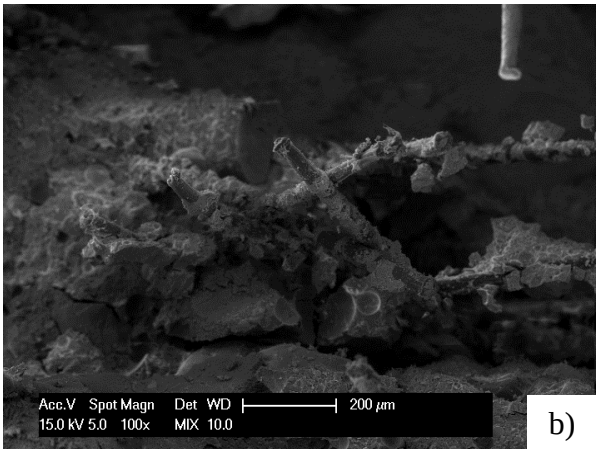

b)

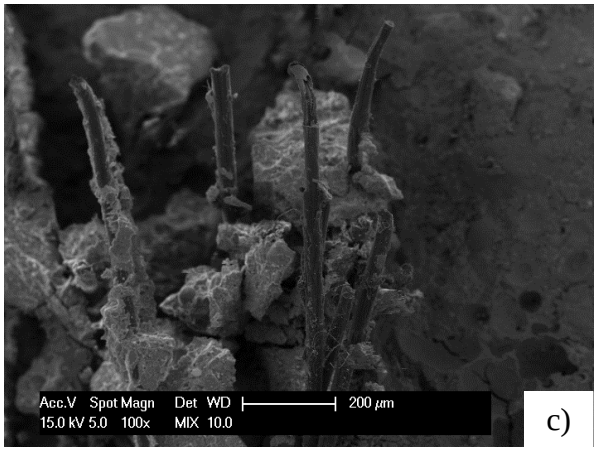

c)

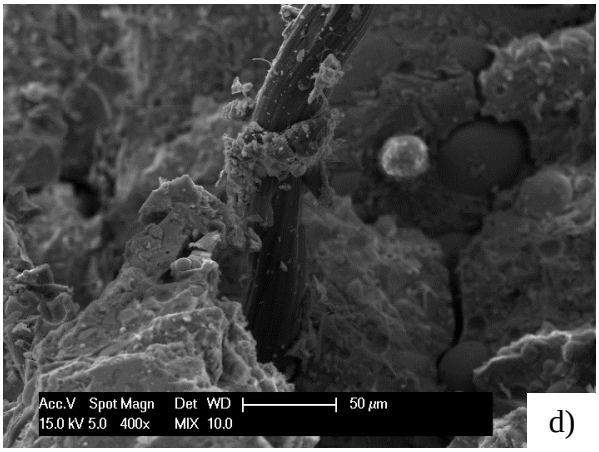

d)

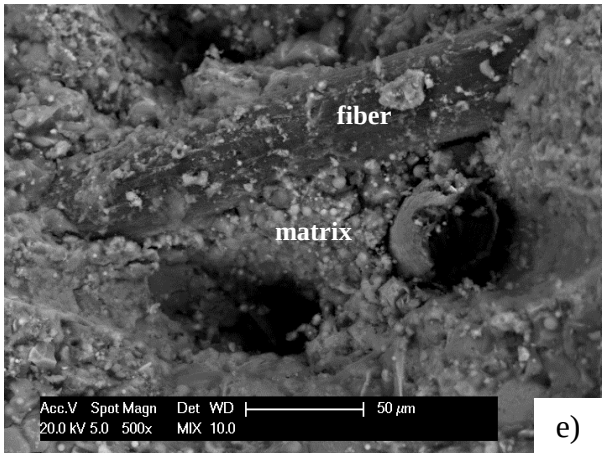

e)

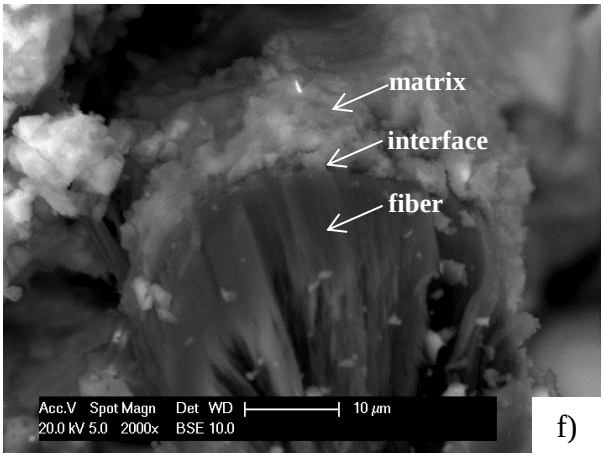

f)

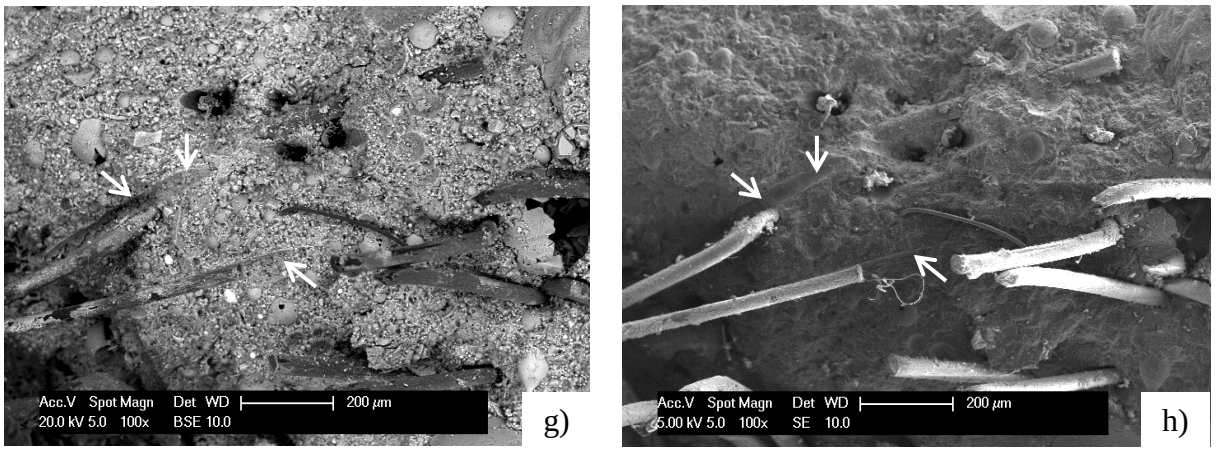

Fig. 14. ESEM micrographs of the fractured samples at 120 days, a), b), c), d), e) MIX mode represents combined SE and BSE modes in which the micrographs of different fiber fracture mechanisms were obtained, a), b) Combined PVA fiber pullout and PVA fiber fracture, showing strong bond between fibers and matrix (after the fracture fibers are still surrounded by **reaction** products), c) and d) Fiber pullout in lower and higher magnification, e) and f) Fiber fracture in lower and higher magnification, g) and h) Combined fiber pullout and fiber fracture, (white arrows indicate fiber imprints) obtained by BSE and SE, respectively.

5. Application – Environmentally friendly, cement free concrete canoe

Many innovative materials are developed in the laboratories but their structural applicatons in the practical projects are scarce. As previously mentioned, reasons for this are numerous: no available codes, difficulties in getting permissions, lack of experience, no confidence in their long-term behaviour, etc. After all, the experience that the practice has with concrete and other construction materials is based on decennia or centuries of applications and "trial projects". In order to gain confidence with the new materials, low risk projects and small scale structural applicatons are perfect oportunites to test the limits of materials and gain the experience for the future applicatons. One such project is the application of the AAM in the canoe for the student competition. In the Netherlands the Concrete Canoe Race, organized annually under the auspices of the Dutch concrete association (Betonvereniging), challenges students of civil engineering to make a concrete canoe. During this event students from different universities and institutions compete in their self-built concrete canoes. The aim of

the event is to promote the multi-purpose use of concrete. The following aspects were considered when designing and constructing the TU Delft Canoe for Beton Kano Race 2016:

(a) Use of a sustainable, environmentally friendly mixture, i.e. the use of AAM concrete.

(b) The canoe should have enough load carrying capacity during unmoulding and exploitation phase (sailing).

(c) Mitigate drying shrinkage cracking in order to ensure watertightness

(d) Avoid brittle failure of the canoe.

In order to satisfy these criteria, the mixture design for the canoe (of the TU Delft Beton Kano Race 2016 team) was developed (mixture described in this paper is used). The principles for shaping and constructing the concrete canoe are determined by the race requirements. In this study, the focus was on the constructing part, which considers satisfying the safety and functionality criteria. First, the canoe has to have proper mortar/concrete mix and reinforcement in order to carry expected loads on the canoe construction (safety criterion). Second, the functional criterion is related to the serviceability and watertightness. From the aspect of the expected forces on the canoe construction, the permanent and variable forces, such as those from the self-weight, weight of the racers (designed load of 200 kg) and the nautical function of the structure are taken into account. Calculations were done in order to check the load bearing strength of the canoe and to determine what is the critical thickness of the canoe. Codes for the traditional concrete are used for the design. It was found that a 15 mm canoe thickness without the reinforcement mesh satisfies the maximum stress criterion. Therefore, canoe thickness of 16 mm obtained during the final canoe manufacturing, satisfied the criterion.

5.1. Applied mixture and casting procedure

Regarding the concrete mixture, the aim was to design an innovative and sustainable alkali-activated material that will satisfy the race regulations. This mixture was used for the first time in such a large scale model. The manufacturing process was challenging since setting time of the AAM mixture was less than 30 minutes (see Table 4).

The actual casting of the canoe was performed by 15 students who casted fibre reinforced alkali-activated composite in a canoe shaped mould (Fig. 3). The final material has to be "strong enough, light enough, and workable" to be able to cast the canoe. The whole process took around 50 minutes: 2 batches were consecutively made, each of them needing 5 minutes for mixing and having around 24 minutes to be cast since that was the initial setting time of the mix. The canoe was made out of two layers. Between the two layers a plastic fiberglass mesh was placed in order to avoid contraction cracks. The thickness of each layer was around 8 mm which resulted in the total thickness of the canoe wall of around 16 mm.

5.2. Structural components of the canoe

The reinforcement in the canoe is provided by the plastic fiberglass watertight mesh and PVA fibres. The mixture composition is given in Table 3. An expanded polystyrene is used in the front and back parts of the canoe to create a hollow space covered by concrete that constitutes the floating bodies, due to its compressive strength and light weight. In the end, the canoe was painted by watertight concrete paint and padding was installed to cover and protect the edges of the canoe. The mass of the finished canoe was 250 kg. It has to be highlighted that this is a heavy construction compared to previous canoes and that, in the future, more work should be done on weight optimization.

5.3. Canoe demoulding

The canoe was sealed for 1 day and subsequently uncovered. Due to the susceptibility of the mixture to early age shrinkage, curing agent (Sikagard-674 Lasur W, based on acrylic

dispersion) was applied. After 3 days of curing, it was demoulded (Fig. 15a). Subsequently, the curing agent was applied at the canoe outer surface. Due to the concentrated loads at the support points due to the large self-weight, the unmoulding procedure was critical and had to be properly prepared and executed.

5.4. Watertightness test

The exterior side of the canoe needs to have minimal permeability so that it can be considered watertight. Watertightness test of the canoe was tested by a trial run, 7 days afer casting. The test was performed in a water canal close to the laboratory (Fig. 15b). Even without being painted by the watertight concrete paint, the canoe successfully resisted the load of two racers (average weight around 80 kg), self-weight and water pressure without showing any signs of water ingress at the interior side of the canoe. The watertightness test and trial ride of the canoe were considered successful and the canoe was further used for the student competition race.

Fig. 15. a) Demoulding the canoe, b) watertightness test and trial ride of the canoe.

5.5. Verification of the developed composite- significance of the application

To the knowledge of the authors, so far there is no literature with respect to the structural applications of fiber-reinforced alkali-activated FA and GBFS. Implementing a rapid

hardening mixture in a large-scale case is challenging, as GBFS rich alkali-activated mixtures tend to harden fast, quickly leading to drying-shrinkage cracking to be observed. Therefore, for a brittle material such as AAM to be applied to a large-scale structural cases there are several important factors to consider.

In this study, the interaction between the matrix, sand, and fibres in the composite was evaluated from the fresh state and the hardened state. From the first aspect, section 4.1 shows that the use of PVA fibres in alkali-activated FA and GBFS mortar was beneficial not only for improved workability but also in delaying the final setting time which enables sufficient time for large batch to be cast sucessfully. In order to avoid cracking due to early age shrinkage, it was of paramout importance that the proper curing is provided. By visual inspections on the surface of canoe, no cracking was observed over a period of 1 year in outdoors conditions, as shown in Fig. 16.

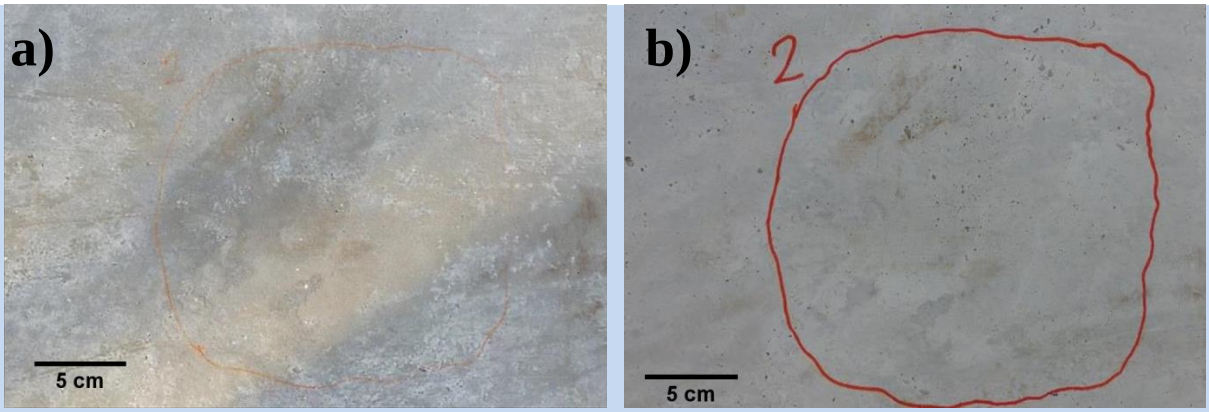

Fig. 16. Inspection of the surface of the canoe a) July 2016; b) May 2017.

From the aspect of the hardened properties, section 4.2 demonstrated good bonding of the matrix with the PVA fibres through testing of the flexural behaviour of fibre reinforced mortar. Still, steps are to be made in future to improve the ductility, for example by using higher strenght fibres. In addition, the properties of a small and a large batches were compared showing an absence of casting scale effect as demonstrated by their similar performances. This ultimately enabled casting of the concrete canoe. Finally, in section 5 it

was shown that the newly developed composite was successfully structurally applied. Furthermore, the incorporation of fibre reinforced AAM in structural applications outside of the laboratory could provide valuable information, provided that the long-term behaviour of the composite in the real-service conditions is monitored and measured.

For the future design of the canoe, several goals are set:

- The weight of the canoe should be reduced by application of light weight aggregate or polystyrene beads.
- Better design of the mould in order to reduce the self-weight and increase the speed of the canoe should be made.
- Considering calculation and gained experience, it is envisioned that even without the mesh reinforcement fibre reinforced mixture would satisfy specified criteria.

These aspects will be tackled at next year's competition, when the structural application of geopolymer, as sustainable material solution for concrete structures, will be further optimized.

6. Conclusions

A fibre reinforced alkali-activated composite was successfully designed and upscaled to large scale production (from 3 l to 45 l). Rheology and mechanical properties were investigated. Alkali-activated composites made in different quantities, i.e. 3 l and 45 l showed similar behaviour, demonstrating an absence of casting scale effect, and the feasibility for large scale applications. The bonding between alkali-activated matrix and fibres is found to be strong enough to resist various mechanical loading, and environmental conditions on canoe after one year of exposure. A combination of fibre pullout and fibre rupture was observed, which finally resulted in the failure of the specimen due to fibre rupture. In order to improve the fracture behavior of fibre reinforced AAM, future efforts will focus on applying fibres with higher strength, such as polyethylene or aramid fibres, previously used for designing HS-SHCC. It is envisioned that fibre reinforced AAM will be especially beneficial for

construction of membrane, thin elements, with preferential fibre orientations where the fibres are optimally utilized. The application of the developed environmentaly friendly material in the canoe has shown promising results and provided significant experience and confidence for further upscaling of this innovative material and its structural application in larger scale projects.

Acknowledgements

This research was carried out under the project S81.1.13498 in the framework of the Partnership Program of the Materials innovation institute M2i (www.m2i.nl) and the Technology Foundation STW (www.stw.nl), which is part of the Netherlands Organisation for Scientific Research (www.nwo.nl). The authors thank Branko Savija, Stefan Chaves Figueiredo, Kamel Arbi, the PhD candidates from Microlab section, students from the the U-BASE student union and TU Delft Beton Kano Race 2016 team for their help and support during casting and the race, and Arjan Thijssen for his help with the ESEM observations. The team has won two awards during the Concrete Canoe Race of 2016, for the heaviest canoe of this year's race and for the most sustainable canoe because of the extraordinary material the canoe was made of.

References

AFGC. 2013. Ultra high performance fibre-reinforced concrete, Recommendations, AFGC Groupe de travail BFUP.

Alcaide, J.S., Alcocel, E.G., Puertas, F., Lapuente, R., Garcés, P., 2007. Carbon fibre-reinforced, alkali-activated slag mortars. Materiales de Construcción, 57(288), 33-48.

Aydın, S., Baradan, B., 2013. The effect of fiber properties on high performance alkali-activated slag/silica fume mortars. Composites Part B. 45(1), 63-69.

Bernal, S., De Gutierrez, R., Delvasto, S., Rodriguez, E., 2010. Performance of an alkali-activated slag concrete reinforced with steel fibers. Constr. Build. Mater. 24(2), 208-214.

Choi, J.I., Song, K.I., Song, J.K., Lee, B.Y., 2016a. Composite properties of high-strength polyethylene fiber-reinforced cement and cementless composites. Compos. Struct. 138, 116-121.

Choi, J.I., Lee, B.Y., Ranade, R., Li, V.C., Lee, Y., 2016b. Ultra-high-ductile behavior of a polyethylene fiber-reinforced alkali-activated slag-based composite. Cem. Concr. Compos. 70, 153-158.

Curosu, I., Mechtcherine, V., Millon, O., 2016. Effect of fiber properties and matrix composition on the tensile behavior of strain-hardening cement-based composites (SHCCs) subject to impact loading. Cem. Concr. Res. 82, 23-35.

Curosu, I., Liebscher, M., Mechtcherine, V., Bellmann, C., Michel, S., 2017. Tensile behavior of high-strength strain-hardening cement-based composites (HS-SHCC) made with high-performance polyethylene, aramid and PBO fibers. Cem. Concr. Res. 98, 71-81.

Dias, D.P., Thaumaturgo, C., 2005. Fracture toughness of geopolymeric concretes reinforced with basalt fibers. Cem. Concr. Compos. 27(1), 49-54.

fib bulletin 65. Model Code 2010, Final draft, Volume 1, federation international du béton (fib), Lausanne, Switzerland, ISBN: 978-2-88394-105-2, 2012.

Jiang, C., Fan, K., Wu, F., Chen, D., 2014. Experimental study on the mechanical properties and microstructure of chopped basalt fibre reinforced concrete. Mater. Des. 58, 187-193.

Kajaste, R., Hurme, M., 2016. Cement industry greenhouse gas emissions–management options and abatement cost. J. Cleaner Prod. 112, 4041-4052.

Lee, B.Y., Cho, C.G., Lim, H.J., Song, J.K., Yang, K.H., Li, V.C., 2012. Strain hardening fiber reinforced alkali-activated mortar–a feasibility study. Constr. Build. Mater. 37, 15-20.

Li, V.C., 2003. On engineered cementitious composites (ECC). J. Adv. Concr. Technol. 1(3), 215-230.

Li, V.C., Stang, H., 1997. Interface property characterization and strengthening mechanisms in fiber reinforced cement based composites. Adv. Cem. Based Mater. 6(1), 1-20.

Li, W., Xu, J., 2009a. Impact characterization of basalt fiber reinforced geopolymeric concrete using a 100-mm-diameter split Hopkinson pressure bar. Mater. Sci. Eng., A. 513, 145-153.

Li, W., Xu, J., 2009b. Mechanical properties of basalt fiber reinforced geopolymeric concrete under impact loading. Mater. Sci. Eng., A. 505(1), pp.178-186.

Li, Z., Ding, Z., 2003. Property improvement of Portland cement by incorporating with metakaolin and slag. Cem. Concr. Res. 33(4), 579-584.

Lothenbach, B., Scrivener, K., Hooton, R.D., 2011. Supplementary cementitious materials. Cem. Concr. Res. 41(12), 1244-1256.

Lukovic, M., 2016. Influence of interface and strain hardening cementitious composite (SHCC) properties on the performance of concrete repairs (Doctoral dissertation, TU Delft, Delft University of Technology).

Luković, M., Šavija, B., Schlangen, E., Ye, G., van Breugel, K., 2016. A 3D lattice modelling study of drying shrinkage damage in concrete repair systems. Materials, 9(7), 575.

Marinković, S., Dragaš, J., Ignjatović, I., Tošić, N., 2017. Environmental assessment of green concretes for structural use. J. Cleaner Prod. 154, 633-649.

McLellan, B.C., Williams, R.P., Lay, J., Van Riessen, A., Corder, G.D., 2011. Costs and carbon emissions for geopolymer pastes in comparison to ordinary portland cement. J. Cleaner Prod. 19(9), 1080-1090.

Mehta, P.K., Monteiro, P. J. M., 2006. Concrete: Microstructure, Properties and Materials. p. 659.

Naaman, A.E., 2007. High performance fiber reinforced cement composites: classification and applications. In CBM-CI international workshop, Karachi, Pakistan (pp. 389-401).

Natali, A., Manzi, S., Bignozzi, M.C., 2011. Novel fiber-reinforced composite materials based on sustainable geopolymer matrix. Procedia Eng. 21, 1124-1131.

Nedeljković, M., Arbi, K., Zuo, Y., Ye, G., 2016. Physical properties and pore solution analysis of alkali activated fly ash-slag pastes. In Proceedings pro113: International RILEM Conference Materials Systems and Structures in Civil Engineering 2016 (MSSCE 2016) on Concrete with Supplementary Cementitious Materials.

Nematollahi, B., Sanjayan, J., Ahmed Shaikh, F.U., 2015. Tensile strain hardening behavior of PVA fiber-reinforced engineered geopolymer composite. J. Mater. Civ. Eng. 27(10), p.04015001.

NEN-EN 196-3: 2005. Methods of Testing Cement. Part 3: Determination of Setting Times and Soundness.

NEN-EN 12350-6: 2009. Testing fresh concrete - Part 6: Density.

NEN-EN 14651: 2005. Test method for metallic fibered concrete-Measuring the flexural tensile strength (limit of proportionality (LOP), residual).

Pacheco-Torgal, F., Labrincha, J., Leonelli, C., Palomo, A., Chindaprasit, P. eds., 2014. Handbook of alkali-activated cements, mortars and concretes. Elsevier.

Palacios, M., Banfill, P.F., Puertas, F., 2008. Rheology and setting of alkali-activated slag pastes and mortars: effect of organic admixture. ACI Mater. J. 105(2), pp.140-148.

Paul, S.C., van Zijl, G.P., 2013. Mechanically induced cracking behaviour in fine and coarse sand strain hardening cement based composites (SHCC) at different load levels. J. Adv. Concr. Technol. 11(11), 301-311.

Provis, J.L., Palomo, A., Shi, C., 2015. Advances in understanding alkali-activated materials. Cem. Concr. Res. 78, 110-125.

Provis, J.L., 2014. Geopolymers and other alkali activated materials: why, how, and what? Mater. Struct. 47(1-2), 11-25.

Puertas, F., Amat, T., Vázquez, T., 2000. Behaviour of alkaline cement mortars reinforced with acrylic and polypropylene fibres. Materiales de Construcción, 50(259), 69-84.

Puertas, F., Amat, T., Fernández-Jiménez, A., Vázquez, T., 2003. Mechanical and durable behaviour of alkaline cement mortars reinforced with polypropylene fibres. Cem. Concr. Res. 33(12), 2031-2036.

Puertas, F., Gil-Maroto, A., Palacios, M., Amat, T., 2006. Alkali-activated slag mortars reinforced with AR glassfibre. Performance and properties. Materiales de Construcción, 56(283), 79-90.

Sakulich, A.R., 2011. Reinforced geopolymer composites for enhanced material greenness and durability. Sustainable Cities and Society, 1(4), 195-210.

Savastano, H., Warden, P.G., Coutts, R.S.P., 2005. Microstructure and mechanical properties of waste fibre–cement composites. Cem. Concr. Compos. 27(5), 583-592.

Scrivener, K.L., Crumbie, A.K., Laugesen, P., 2004. The interfacial transition zone (ITZ) between cement paste and aggregate in concrete. Interface Sci., 12(4), 411-421.

Shah, S.P., 1992. Do fibers increase the tensile strength of cement-based matrix? ACI Mater. J. 88(6), 595-602.

Silva, F.J., Thaumaturgo, C., 2003. Fibre reinforcement and fracture response in geopolymeric mortars. Fatigue Fract. Eng. Mater. Struct., 26(2), 167-172.

Worrell, E., Price, L., Martin, N., Hendriks, C., Meida, L.O., 2001. Carbon dioxide emissions from the global cement industry. Annu. Rev. Energy Env. 26(1), 303-329.

Zhang, Z., Yao, X., Zhu, H., 2010. Potential application of geopolymers as protection coatings for marine concrete: II. Microstructure and anticorrosion mechanism. Appl. Clay Sci. 49(1), 7-12.

Zhang, Z., Yao, X., Wang, H., 2012. Potential application of geopolymers as protection coatings for marine concrete III. Field experiment. Appl. Clay Sci. 67, 57-60.

Zhou, J., Qian, S., Beltran, M.G.S., Ye, G., van Breugel, K., Li, V.C., 2010. Development of engineered cementitious composites with limestone powder and blast furnace slag. Mater. Struct. 43(6), 803-814.

List of figures:

6. Fig. 6. Flexural strength of the pastes, mortar and fibre reinforced mortar based on alkali- activated FA and GBFS, measured by three-point bending test on samples 40x40x160 mm^3.
7. Fig. 7. Flexural load-displacement curves for 3litres (black) and 45 litres (grey) after different ages (1, 3, 7, 28 and 120 days).
8. Fig. 8. Crack patterns for mix 3 litres (left) and mix 45 litres (right) after 7 days of curing on samples tested in four-bending test.
9. Fig. 9. The flexural strength of the 3 litres and 45 litres samples (10x30x120 mm^3), measured by four-point bending tests.
10. Fig. 10. Flexural deflection capacity at the maximum load (defined according to Fig. 3) as a function of time for batches of 3 litres and 45 litres.
11. Fig. 11. Flexural tests on (a) 100x100x400 mm^3 notched samples (left) and (b)10x30x120 mm^3 notched samples (right) made from 45 litres batches at 7d and 120d.
12. Fig. 12. Crack patterns at the notch after three-point bending test for mixture 45 litres at 7d and 120d.
13. Fig. 13. Optical micrographs of the fractured samples at 120 days a) Top surface of the fractured sample (0.63x magnification), b) Fiber pullout and fiber-matrix debonding (2x magnification, c) Fiber pullout magnified (4x magnification), d) Fiber bridging and fiber-matrix debonding (4x magnification).
14. Fig. 14. ESEM micrographs of the fractured samples at 120 days, a), b), c), d), e) MIX mode represents combined SE and BSE modes in which the micrographs of different fiber fracture mechanisms were obtained, a), b) Combined PVA fiber pullout and PVA fiber fracture, showing strong bond between fibers and matrix (after the fracture fibers are still surrounded by hydration products), c) and d) Fiber pullout in lower and higher

List of tables: